KINEMATICS OF A FREE PITCHING FLEXIBLE CANTILEVER NACA 0012 AIRFOIL WITH STRUCTURAL AND AERODYNAMIC NON-LINEARITIES AT TRANSITIONAL REYNOLDS NUMBERS

Crystal Itwar Barrett, MASc. Candidate
Department of Mechanical and Aerospace Engineering
Royal Military College of Canada
Kingston, Ontario, Canada
Crystal.Itwar-Barrett@rmc.ca

Dr. Dominique Poirel
Department of Mechanical and Aerospace Engineering
Royal Military College of Canada
Kingston, Ontario, Canada
poirel-d@rmc.ca

Dr. Asad Asghar
Department of Mechanical and Aerospace Engineering
Royal Military College of Canada
Kingston, Ontario, Canada
Asad.Asghar@rmc.ca

I. INTRODUCTION

The dynamics of a free pitching flexible cantilever NACA 0012 airfoil were investigated at transitional Reynolds numbers. It is well noted that the aerodynamics at transitional Reynolds numbers are complex, and include such phenomena as laminar boundary layer separation, which may subsequently form a laminar separation bubble (LSB) [1].

This work builds on previous investigations based on a quasi-2D rigid wing, moving elastically in pitch and heave. In this current experimental investigation, the wing testing apparatus consisted of the flexible cantilever NACA 0012 wing, mounted over a thin steel beam. The wing/beam combination was mounted on a free rotating base. The free rotary base that holds the beam is connected to translational springs on a pulley. The beam provided the structural stiffness, while the wing provided the aerodynamic loads.

This set-up enabled the study of the coupling between rigid body modes (flight dynamics) and flexible modes (aeroelasticity). Furthermore, it would provide a means to study the effect of the expected non-linearities: aerodynamic (flow separation due to a combination of large angle of attack and transitional Reynolds number) [2] and geometric (due to large displacement and mainly non-linear pitch-bending coupling) [3].

II. INSTRUMENTATION AND SET-UP

Fig. 1 illustrates the locations of the quarter chord point (c/4), centre of gravity (C.G.), elastic axis (E.A.) and pitch axis (P.A.) for the system. Note that in our case, the P.A. coincides with the E.A.

Pitch data was measured using a contactless potentiometer: the Contelec Co-Vert-X 22E2 836 221 505 78107 1307 1. This was used to capture small amplitude oscillations (SAO) and large amplitude oscillations (LAO), which will be further discussed in section IV.

The beam was outfitted with two PCB Piezoelectronics 352C22 accelerometers and eight Vishay EA-06-240LZ-120 strain gauges (four for bending and four for torsion) (see Fig. 2). The strain gauges were applied in a four-arm bridge configuration, such that temperature, axial and torsional components were compensated for the bending strain gauges, and torsion strain gauges were sensitive to torsion only [4]. The data from the accelerometers fed into a PCB 483C signal conditioner. The strain gauge data fed into a model 2120 Strain Gauge signal conditioner. The conditioned strain gauge and accelerometer data, along with the potentiometer data, fed into the National Instruments cDAQ 9174, which connected to the computer and LabVIEW via USB; see Fig. 3.

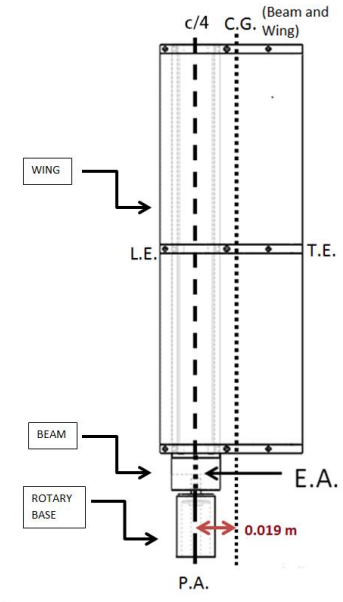

Figure 1. Relevant System Axes

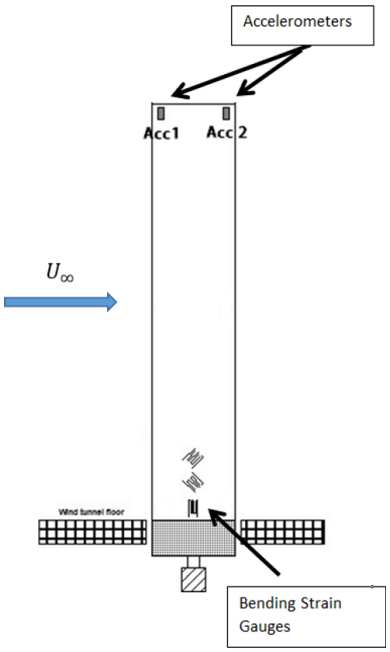

Figure 2. Bending Strain Gauge and Accelerometer Positions

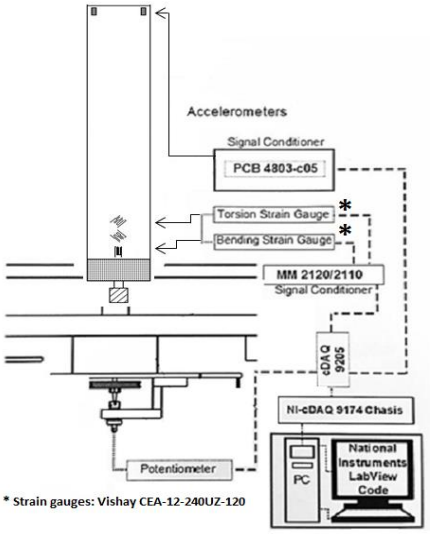

Figure 3. Experimental Test Set-Up

No-flow data was used to find the mean bias of the wing, as well as estimate filtering frequencies based on the noise characteristics. Furthermore, performing no-flow tests before and after testing provided a means to check if the system parameters had changed.

No flow testing was also crucial for determining the structural properties of the system by performing free decay tests for each of the three configurations: S1 (rotary base, shaft, pulley, and encoder), S2 (rotary base, steel beam, eight strain gauges, two accelerometers, wires, shaft, pulley, encoder, and adhesives), and S4*(rotary base, steel beam, NACA 0012 wing, eight strain gauges, two accelerometers, wires, shaft, pulley, encoder, and adhesives) configurations as seen in Fig. 4-6, respectively. This data would allow us to find the decay rate and damping coefficient of the system.

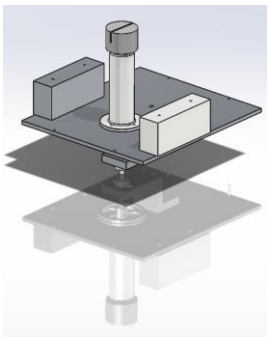

Figure 4. S1 Configuration (Rotary base only)

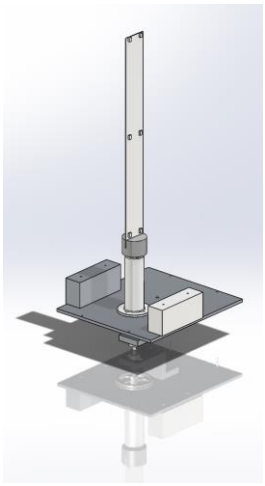

Figure 5. S2 Configuration (Rotary base and beam)

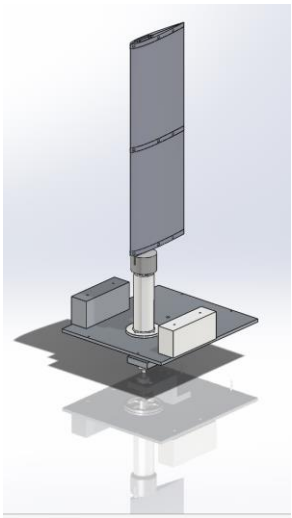

Figure 6. S4* Configuration (Rotary base, beam and wing)

III. METHODOLOGY

The experimental data obtained was recorded using LabVIEW and 1000 Hz sample rate (to ensure that at least the first two modal frequencies would be captured).

Prior to testing, the ambient conditions were recorded and no flow tests were performed. Then, the airspeed was increased until a limit cycle oscillation (LCO) [5] was observed. The data was recorded individually for several airspeeds. In an effort to locate the LCO branches, initial conditions were applied to the wing in the form of pitch perturbations and changes in airspeed. Post-test no flow tests were performed once all relevant data was collected. Airspeed measurements were recorded by means of a pitot static tube and data was recorded when steady-state was attained for a given airspeed.

The S1 configuration was used to determine the moment of inertia of the base, and damping coefficient in pitch. The S2 configuration was used to determine the moment of inertia of the beam and rotary base.

The 1st and 2nd analytical natural frequencies were calculated for bending and torsion of the S2 configuration (based on elastical beam theory), and the pitch damped natural frequency was experimentally determined for the S2 configuration as well, as seen in Table I.

TABLE I.
NATURAL FREQUENCIES (S2 CONFIGURATION)

Natural Frequencies (Hz) based on [6],[7],[8],and [9]		
Motion	***Mode 1***	***Mode 2***
Pitch	5.3	n/a
Bending	6.0	38
Torsion	102	308

Note that for the S2 configuration the bending and torsion modes (as defined by the motion of the EA) are uncoupled due to the beam uniformity. The pitch motion is also considered to be uncoupled from the torsion motion due to the large difference in frequency scale. This assumption was confirmed from results of a finite difference (FD) solution of the S2 configuration (Table I).

For the S4* configuration, the bending and torsion are coupled due to the static imbalance (i.e. C.G. and E.A. are not coinciding). FD modeling of the S4* configuration resulted in the first three modes at 2.56 Hz, 5.0 Hz and 29.4 Hz. These numerical results also match those obtained from the no flow tests (equivalent to ground vibration testing (GVT) for full-scale aircraft). The first mode is pitch dominated, and the second mode is bending dominated.

IV. RESULTS AND DISCUSSION

Data was plotted for the potentiometer, strain gauges, and accelerometers, illustrating the LCO branches. However, only the first few points of the LAO region were plotted since it was suspected that strain hardening occurred at higher airspeeds.

A. Potentiometer (Amplitude of Root Pitch Angle) Results

Values of the mean positive peak amplitude of the root pitch angle were plotted versus airspeed (Fig. 7). It is worthy to confirm that the range of airspeeds corresponded to a Reynolds number range of $7.93 \times 10^4 < Re_c < 1.11 \times 10^5$, which is indeed in the range of transitional Reynolds numbers. Previous research has observed that the range of Reynolds numbers where LCO's occur is $5.5 \times 10^4 < Re_c < 1.2 \times 10^5$ [2]. Hitherto for the quasi-2D rigid wing, elastically mounted in pitch and heave, two LCO regions (also called branches) had been observed [2]. These regions can be described as SAO and LAO. Another interesting observation is that the onset of LCO (and the beginning of the SAO region) is at approximately 8 m/s. The onset of LAO appears to occur at just below 9 m/s.

Referring to Fig. 6, the SAO and LAO branches are clearly evident and are tentatively defined as the ranges of 0^0-15^0, and 30^0-60^0 for SAO and the commencement of LAO, respectively. Sample time traces showing a few cycles of the root pitch SAO (Fig. 8) and root pitch LAO (Fig. 9) are shown. These values were found by means of performing a simple physical calibration using a protractor to relate voltage to degrees.

It is important to note that the LAO region across all tests did not appear to be stationary, or at steady state, i.e. there was significant amplitude modulation (as seen in Fig. 9). No explanations are offered at this time. Preliminary tests also showed evidence of a possible third branch of very large oscillations (VLAO), in the range of 80°-120°; however, the existence of this branch was debunked with this current experimental investigation, which confirmed that the possible VLAO region was simply due to a spring extension issue in the apparatus.

Moreover, the positive and negative mean peak amplitudes of the root pitch angle were not symmetrical for all tests, which was likely an artefact of the wing oscillating about a slightly non-zero position due to inherent asymmetries: deviating flow, the wing pitch axis not being entirely aligned with the flow, and wing warp/asymmetries.

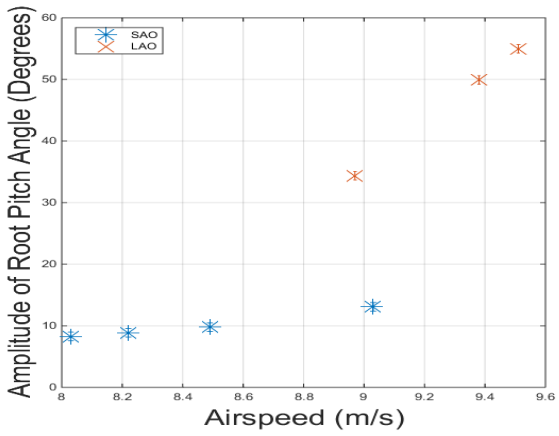

Figure 7. Amplitude of Root Pitch Angle Versus Airspeed

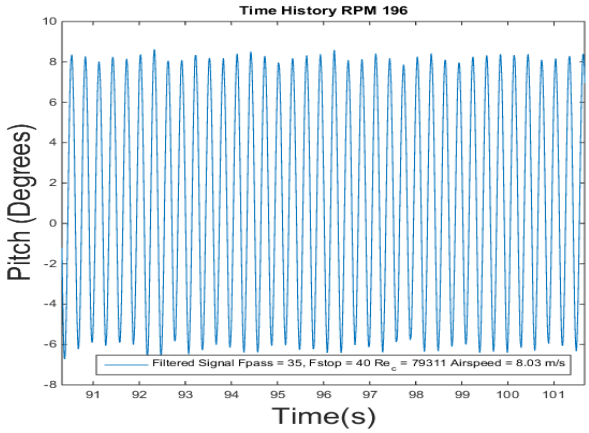

Figure 8. Root Pitch Angle Versus Time (SAO)

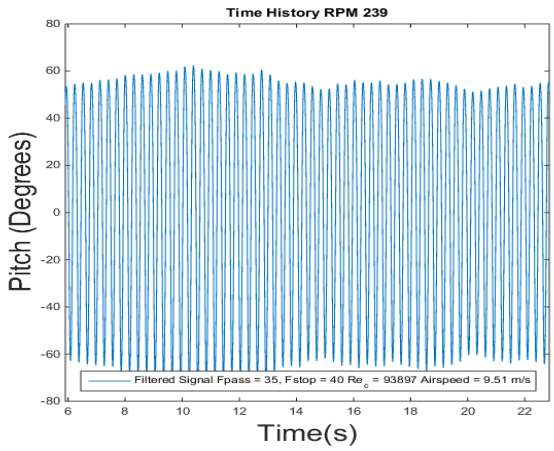

Figure 9. Root Pitch Angle Versus Time (LAO)

While we theorize that SAO is caused by laminar flow separation, in a feedback relationship with the free pitching wing motion which causes negative aerodynamic damping, the physical mechanisms which cause LAO are still to be confirmed. Hence, LAO will be the primary focus, with the SAO serving to confirm that the Reynolds number effect is present, which provides information on the state of the flow. For our testing, the existence of the Reynolds number effect confirms that the flow is laminar.

It is meaningful to state that the wing could possibly be experiencing coalescence flutter and dynamic stall for the LAO branch, the latter of which is one of several non-linearities that limits the oscillation amplitudes. For the possibility of coalescence flutter, this could be a result of the coupling of the pitch and 1st bending mode as these two frequencies are close to each other (Table IV). This preliminary review of pitch data is important because we use it as a guide; if we ascertain that it is well behaved, we thusly assume that the bending, torsion and acceleration data will also be well behaved.

As a corollary, two qualitative tests were performed wherein the pitch motion was locked, allowing only bending-torsion motion. The airspeed was gradually increased to over 12 m/s, however, no coupling between the bending dominant mode and torsion dominant mode was observed. Hence, qualitatively, this further suggested that there is a coupling between the pitch dominant mode (rigid body mode) and 1st bending dominant mode (flexible body mode). Furthermore, this is congruent with the data in Table I, which indicated that there would be no expected coupling between the pitch dominant and torsion dominant modes.

B. Strain Gauge (Amplitude of Tip Bending Deflection) Results

The tip bending deflection for the SAO and LAO regions is presented (Fig. 10). In Fig. 10, there are two clear branches present, illustrating a ranges of 2.0-8.0 cm, and 14-22 cm bending deflection for the SAO and commencement of LAO regions, respectively. Fig. 11 is a sample time trace of the bending deflection. Analytical comparison illustrated that the 1st mode shape of vibration of a homogeneous cantilever beam (for a linear system) closely approximates the shape of the beam when a point load is applied at the tip. Hence, the aforementioned assumption meant that deflection values could be found by means of performing a simple physical calibration to relate strain gauge voltage to deflection at the tip using a specially made in-house calibration jig.

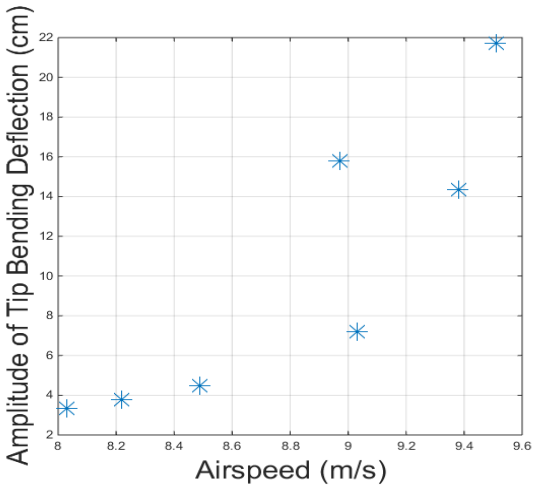

Figure 10. Amplitude of Tip Bending Deflection Versus Airspeed

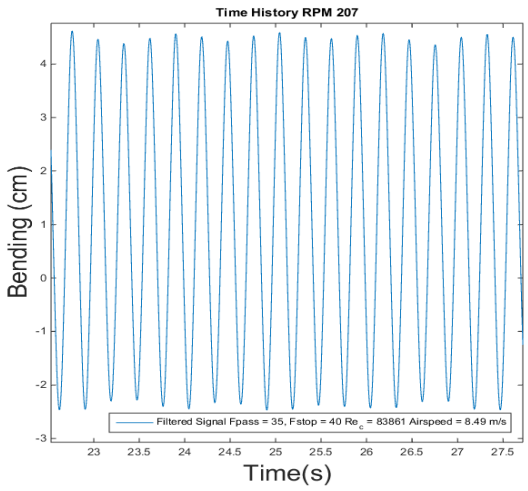

Figure 11. Tip Bending Deflection Versus Time (SAO)

C. Accelerometer (Amplitude of Total Tip Acceleration) Results

The analysis of the accelerometer data yielded tip accelerations at positions indicated in Figure 2, and can be seen in Fig. 12. In general the acceleration range for accelerometer 1 in the SAO region is 16-32 m/s^2; whereas, for accelerometer 2, the acceleration range is 4.0-18 m/s^2. For the commencement of the LAO region, the ranges are 50-60 and 35-45 m/s^2, for accelerometers 1 and 2, respectively. While this suggests higher loads experienced towards the wing L.E, further analysis is required. Fig.13 is a sample time trace of the acceleration data. Conversion from voltage to m/s^2 was done by using the manufacturer provided calibration values for each specific accelerometer serial number.

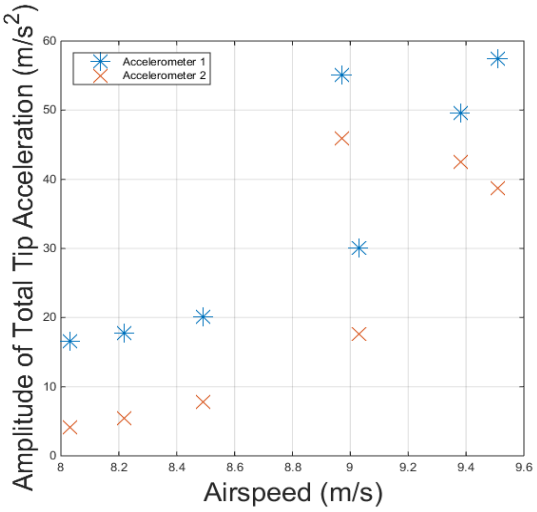

Figure 12. Amplitude of Total Tip Acceleration versus Airspeed (Accelerometers 1 and 2)

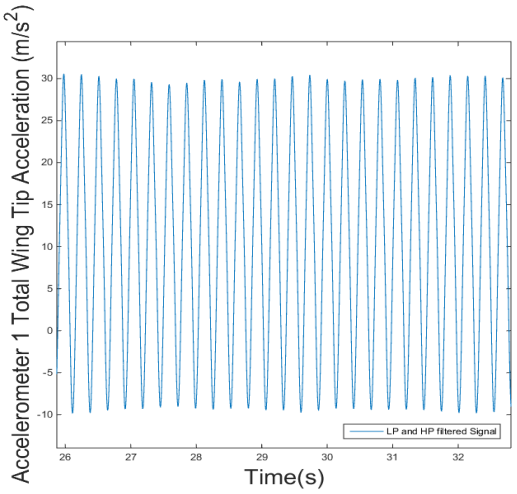

Figure 13. Total Tip Acceleration Versus Time(Accelerometers 1)

D. LCO Frequency Results

The LCO frequencies as measured from the root pitch angle were also found, and shown in Fig. 14. As expected, they match the acceleration and strain LCO frequencies. For the LCO frequency behaviour (Fig. 14), an average frequency resolution $f = 1/F_s\Delta t = 0.0305$ Hz was used, since Δt varied for each test. The experimental values were normalized by using the 1st modal frequency for the S4* configuration (See III Methodology), assuming that this is the mode that becomes unstable first. It was noted that the LCO reduced frequencies (k) range was from 0.13 to 0.15, which indicated that unsteady aerodynamics effects are important.

From Fig. 14, we see that once again, there are two distinct branches, corresponding to SAO and commencement of LAO. All normalized LCO frequencies are within the small frequency spectrum of 1.25-1.5. Note that these are lower than

the normalized uncoupled pitch natural frequency for the S2 configuration (Table I) of approximately 2.07.

Consider that the work from the quasi-2D wing [2] observed that the SAO had an approximate normalized frequency range of 1.09-1.33, whereas LAO had an approximate normalized frequency range of 1.45 – 1.48 (for a frequency ratio of 1.63). Conversely, the results in Fig. 14 indicate a frequency range of approximately 1.25-1.5 for both SAO and LAO, which falls in between the SAO and LAO frequency range based on the quasi-2D wing results mentioned above. Further testing is required to investigate this behavior, especially at higher airspeeds.

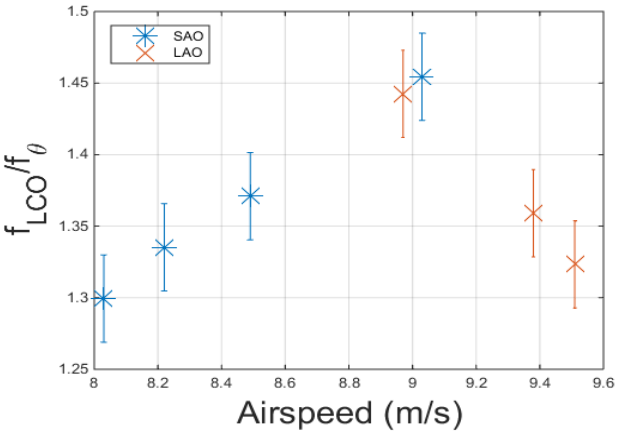

Figure 14. Pitch Angle LCO Frequency Versus Airspeed

V. CONCLUSIONS AND RECOMMENDATIONS

A series of wind tunnel tests were performed with a free pitching cantilever wing, in the transitional Reynolds number region. These tests allowed the study of the coupling between rigid body mode and flexible modes, as well as aerodynamic and geometric non-linearities.

Results were gathered in the range of $7.93 \times 10^4 < Re_c < 1.11 \times 10^5$. Based on the root pitch angle data, LCO branches were evident and tentatively defined as the ranges of 0^0-15^0, and 30^0-60^0 for SAO and the commencement of LAO, respectively. It is theorized that that SAO is caused by laminar flow separation, and LAO is possibly caused by coalescence flutter and dynamic stall.

The tip bending deflections were 2.0-8.0 cm for SAO, and 14-22 cm for LAO. In the SAO region, the tip accelerations were 16-32 m/s^2 and 4.0-18 m/s^2, for accelerometers 1 and 2, respectively. Whereas, in the LAO region, the tip accelerations were 50-60 m/s^2 and 35-45 m/s^2, for accelerometers 1 and 2, respectively. All normalized LCO frequencies are within the small frequency spectrum of 1.25-1.5.

While this work provides a good basis in the ongoing research to characterize the dynamics of a free pitching flexible cantilever NACA0012 wing, more detailed work is required.

The beam material will be revised to increase the yield strength above such that failure occurs in greater than 10^4 cycles, while maintain its current modulus of elasticity. Further tests will be done, and data re-examined in the future, especially at higher airspeeds as we suspect strain hardening is occurring.

The acceleration data will be calibrated in terms of engineering units, i.e. velocity and displacement and compared with the strain gauge deflections; further post-work calculations will also include assessing the damping and stiffness values and flutter speed prediction.

The amalgamation of all results will yield an illustration of the motion of the wing due to the complex physics which occur at transitional Reynolds numbers.

ACKNOWLEDGMENTS

The authors gratefully acknowledge the help and support of Dr. Azemi Benaissa, Dr. David DuQuesnay, M. Lavoie, Brendan Freeman, Jeff Fleming, Charles Sadiq, Pierre Seguin, Pierre Bissonnette, David Babcock, Corey Sharpe and Jason Pell. They also gratefully acknowledge the financial support of the Department of National Defense of Canada (DND), as well as Natural Sciences and Engineering Research Council of Canada (NSERC).

REFERENCES

[1] D. Poirel, Y. Harris, and A. Benaissa. Self-sustained aeroelastic oscillations of a NACA 0012 airfoil at low-to-moderate Reynolds numbers. Journal of Fluids and Structures, Vol. 24, No.5, pp. 700-719, 2008.

[2] D. Poirel and F. Mendes. Experimental small amplitude self-sustained pitch-heave oscillation at transitional Reynolds numbers. AIAA Journal Vol.52 No.8, pp.1581-1590, August 2014.

[3] Robinson, B. (August 2018). Aeroelastic oscillations of a pitching cantilever with structural geometric nonlinearities: theory, numerical simulation and global sensitivity analysis. (Master of Applied Science in Civil Engineering). Carleton Univserity, Ottawa, Canada.

[4] T.G. Beckwith, R.D. Marangoni, J.H. Lienhard V. Mechanical Measurements. Pearson Education. Sixth Edition. pp. 455.

[5] E.H. Dowell, J.Edwards, T.Strganac. Nonlinear aeroelasticity. Journal of Aircraft Vol.40, No.5, pp.857-874, September-October 2003.

[6] A. Bedford and W. Fowler. Engineering mechanics statics and dynamics. Prentice Hall, Upper Saddle River, New Jersey 07458, 2002

[7] D.H Hodges, and G. Alvin Pierce. Introduction to structural dynamics and aeroelasticity. Cambridge university press 40 west 20th street, New York, NY. 10011-11-4211, USA, pp. 35-36, 2002

[8] P.P. Benham, R.J. Crawford, and C.G. Armstrong. Mechanics of engineering materials. Pearson Education Limited, Longman Group Limited ©, pp.115-116, 1996.

[9] W.H. Thomson. Theory of vibration with applications. Prentice Hall Inc. Englewood Cliffs N.J., pp. 273, 1972.